



Investigation of incessant road failure in parts of Abeokuta, Southwestern Nigeria using integrated geoelectric methods and soil analysis

S. A. Ganiyu¹ · M. A. Oladunjoye² · M. O. Olobadola¹ · A. P. Aizebeokhai³ · B. S. Badmus¹

Received: 10 February 2020 / Accepted: 20 January 2021 / Published online: 6 February 2021
© The Author(s), under exclusive licence to Springer-Verlag GmbH, DE part of Springer Nature 2021

Abstract

A flexible pavement devoid of discontinuities allows for smooth movement of a vehicle load on the roadway. This study involved the use of integrated geoelectric methods comprised of 1D and 2D Electrical Resistivity Tomography (ERT) as well as soil analysis to investigate causes of unceasing road failures along busy Camp—Alabata Road, Abeokuta, Southwestern Nigeria. Four road sections (two failed portions and one fair section and one good section) were identified along which four resistivity traverses were established along the investigated roadway. Four 1D Vertical Electrical Sounding (VES) points were also carried out on the 2D ERT lines. Apparent resistivity data were measured along the four traverses using Schlumberger and Wenner arrays with the aid of a Campus Ohmega resistivity meter. The VES and 2D resistivity data were processed and inverted using WinResist and RES2DINV softwares, respectively. Twenty soil samples at a sampling depth (0–1.0 m) with an interval of 0.2 m were also collected on all designated road sections and analyzed for selected hydraulic/geotechnical properties related to pavement durability. Penetration resistance (PR) was measured in situ by a penetrometer while other subgrade soil properties were evaluated in the laboratory. The VES results delineate three geoelectric layers comprising topsoil, weathered basement (clayey), and fractured/fresh basement with their corresponding resistivity values ranging between 71 and 282 Ωm , 12–76 Ωm , and 261–10,094 Ωm . The thicknesses range between 0.9 and 3.2 m for topsoil and 4.5–19.1 m for weathered basement. 2D resistivity inverted sections delineate two lithologic layers: topsoil with resistivity values $> 200 \Omega\text{m}$, devoid of linear geological structures as competent topsoil on a stable road section while incompetent topsoil on failed road sections were characterized by resistivity values $< 200 \Omega\text{m}$. The weathered layers as depicted by 2D inverted resistivity sections were generally of resistivity less than 100 Ωm while fractured/fresh basement were not depicted in the 2D model. Failed road sections are underlain by topsoil with a resistivity ($< 200 \Omega\text{m}$), shallow weathered (clayey) layer, and differential settlement of saturated subgrade materials. Soil analyses results showed that the stable portion depicts lowest mean values of plasticity index (5.12%) and liquid limit (22.21%), uniform sandy-loam textural class, highest mean value (1.24 cm/h) of saturated hydraulic conductivity (K_{sat}); % sand content (73.2%) and Penetration Resistance (PR) values that increased within the sampling depth (0–40 cm). However, one of the failed sections had lowest mean value (0.81 cm/h) of K_{sat} , % sand content (64.9%) and PR values that decreased within the sampling depth (0–40 cm). Analysis of variance (ANOVA) showed that there were significant differences at the 5% level among all designated road sections with respect to percent silt and moisture content (MC). Adequate engineering construction approaches should be adopted considering the thick layer of incompetent formation (clay) observed across the area investigated. Integrated interpretations present a better resolution and detailed characterization of the substratum underlying the pavement.

Keywords Depth · VES · 2D resistivity tomography · Pavement · Subgrade · Hydraulic

Introduction

Available modes of transportation in a particular country allow ease of mobility of people and freight from one place to another. The modes of transportation commonly in use in most parts of the world are road, air, rail, and sea. Road

✉ S. A. Ganiyu
adekunsu@yahoo.com

Extended author information available on the last page of the article

transportation can be regarded as the most visible transportation mode that several peoples in different regions of the world used most on a daily basis. Road networks also manifest as major visible infrastructural projects that show the extent of the physical infrastructural development of a country, major determinant of social functioning of society, and index of national economic advancement (Jegede 2000; Osinowo et al. 2011; Adiat et al. 2017).

The road networks in Nigeria are divided into three different trunks with the responsibilities of construction, maintenance, and rehabilitation being shared by central, state, and local government authorities. Existence of a good road network is a pre-requisite for buoyant economic growth and technological advancement of a nation as it provides a sustainable channel for agricultural production and easy movement of goods and services (Jegede 2000). Road failure can be defined as the inability of pavement to meet its expected design life and satisfactory provision of fundamental services for which it was constructed due to the formation of surface distresses, such as cracks, depressions, potholes, waviness/corrugation, rutting, and erosion (Kumar and Gupta 2010; Onuoha and Onwuka 2014; Okpoli and Bamidele 2016; Žiliūtė et al. 2016; Zou et al. 2017; Peter et al. 2018).

The persistent occurrence of road failure is a common eyesore on many road networks in several parts of Nigeria. Many roads constructed by the government exhibit surface distresses or depressions, an indication of road failure within a relatively short time of usage by the populace. The establishment of the Federal Road Maintenance Agency (FERMA) and several state-owned road maintenance agencies to address issues of road failures by engaging in reconstruction and continuous maintenance did not ameliorate the state or condition of many Nigerian roads. Several road segments in various parts of the country still record incessant failure (Oni and Olorunfemi 2016). Road failures can occur due to many added factors such as high traffic volume, lack of/inadequate maintenance, poor drainage system, vehicle load, poor construction practices, variation in climate, and lack/inadequate knowledge of subsurface geologic materials on which the roads are built (Kiehl and Briegleb 2011; Osemudiamen 2013; Xu and Sun 2013; Žiliūtė et al. 2016; Adiat et al. 2017). Environmental factors such as air temperature, moisture content of subgrade layers, and the sun's intensity, not only influence variation in asphalt pavement strength, but also contribute to early deterioration and inadequate durability of pavements (Hall and Croveti 2007; Adabanija et al. 2016; Vaitkus et al. 2019; Zheng et al. 2019). However, the influence of geological setting on pavement durability is not usually considered and recognized at the design and construction stages (Adabanija et al. 2016; Olofinyo et al. 2019).

Apart from the general discomfort associated with driving on failed roads, different traffic hazards can also arise

as a result of road failure. Among the noticeable traffic hazards encountered by people as a result of road failures are accident, increase in faulty vehicles, waste of valuable time, traffic congestion as well as an adverse effect on the national economy (Jegede 2000; Osinowo et al. 2011; Oni and Olorunfemi 2016).

Because every engineering structure in any form is seated on natural geologic earth materials, adequate knowledge about the subsurface conditions will improve the durability and stability of the constructed edifices, road and highway (Soupios et al. 2007; de Freitas 2009; Osinowo et al. 2011; Adeyemo and Omosuyi 2012; Okpoli and Bamidele 2016; Oyeyemi et al. 2017).

A pavement system consists of three layers (surface course, base, and subbase) of manufactured materials with different thicknesses placed on top of residual soil. Pavement quality is a major concern to road users (vehicle owners and transportation workers), where the pavement thickness and characteristics subgrade layer are the key items related to in situ pavement conditions (Yuejian et al. 2008; Adabanija et al. 2016). The natural soil layer is an inherent part of the pavement structure design and thus has effects on the performance of a pavement (Wu and Sargand 2007). The stability of a pavement structure not only depends on the thickness of the pavement coating but also on the soil support abilities of the subgrade on which the pavement was built (Omisore et al. 2016). The performance of pavement depends greatly on the strength and compactness of the topsoil layer under controlled conditions of both natural moisture content and maximum dry density (Chukka and Chakravarthi 2012). Geotechnically, the presence of excess amounts of fine particles and a high value of liquid limit, with a very low CBR value, promote failure of pavement (Jegede 2000). Residual soil factors which affect the long term performance of road pavement that are worth considering include the heterogeneous nature of subgrade, the existence of linear geological structures such as faults, the presence/absences of expansive clays, and the bearing capacity of the residual soil (Ajayi 1987; Mesida, 1987; Adeleye 2005; Momoh et al. 2008; Singh et al. 2016; Adiat et al. 2017).

Measurement of soil penetration resistance can be used as an index of soil compaction status (Vanags et al., 2004) as it affects trafficability status of a soil. Soil stiffness (strength) has an inverse relationship with penetration resistance (PR). The soil stiffness required to sustain a given surface load decreases as depth increases (Wu and Sargand, 2007). Thus, there is a need to measure the strength property of subgrade material upon which the pavement was built (Livneh and Ishai 1987; Adabanija et al. 2016).

Geophysical methods allow detection of near surface materials and linear geological structures such as fractures and faults beneath the ground surface (Gardi et al. 2017). The electrical resistivity method provides a good means of

detailed study of vertical movement of water in the unsaturated zone, detecting changes in soil moisture content, and determination of depth to the water saturation zone (Benderitter and Schott 1999; Doser et al. 2004). The electrical resistivity of a residual soil depends on several soil properties such as soil structure, texture, porosity, bulk density (BD), moisture content (MC), salinity, and mineralogical content (Samouëlian et al. 2005; Dafalla and Al-Fouzan 2012; Oyeyemi et al. 2017). The 1D resistivity method, otherwise known as Vertical Electrical Sounding (VES), detects vertical variations of subsurface layer resistivity with depth while 2D ERT detects both lateral and vertical variations in electrical resistivity of subsurface structures. Scientists have employed the electrical resistivity method in environmental studies such as detection/delineation of near surface strata, detection of cavities and sinkholes, geotechnical studies/assessment of ground condition, and investigation of structures like earth dams (Fehdi et al., 2011; Shaaban et al. 2013; Hebbache et al. 2016; Camarero and Moreira 2017; Ezersky et al. 2017; Oladunjoye et al. 2017; Oyeyemi et al. 2017). The 2D ERT was also used in the assessment of depth of oil contaminated soil by Abdullah et al. (2014). The importance of corroborating geophysical results with geotechnical analysis of engineering structures cannot be over-emphasized (Osinowo et al. 2011; Okpoli and Bamidele 2016; Gardi et al. 2017; Oladunjoye et al. 2017; Oyeyemi et al. 2017). Moreover, the heterogeneous nature of subsoil necessitates detailed geophysical and soil analysis of subgrade soil. The use of integrated methods to study road failures are well documented (Saarenketo and Scullion 2000; Oladapo et al. 2008; Maslakowski et al. 2014; Mocnik et al. 2015; Adebisi et al. 2016; Ozegin et al. 2016; Adesola et al. 2017; Ezersky and Eppelbaum 2017). In this study, the electrical methods involving VES and 2D ERT as well as soil analyses were integrated to investigate causes of road failure along the Camp–Alabata road linking two federal establishments. The specific objectives were delineation and characterization of subsurface materials underlying the pavement, identify the presence or absence of near geological structure, and evaluation of selected hydraulic/geotechnical properties of subgrade layers.

Site Description, Climate and drainage pattern.

The study area is along the Camp–Alabata road situated within Abeokuta in the southwest part of Nigeria. The road serves as a linking road for two federal establishments which are the Ogun–Oshun River Basin Development Authority (ORBDA) and the Federal University of Agriculture (FUNAAB). The Camp–Alabata road is about 5 km long and was initially constructed in 1987. The road underwent recent reconstruction work in 2010. The general overview showing the state of the section of the road is shown in Fig. 1. The common palliative rehabilitation measures normally seen on this road are the filling of failed

road portions with granites and asphalt piles. It lies within Latitudes 7°11'30"–7°12'15" North of the equator and Longitudes 3°26'15"–3°26'30" East of the Greenwich meridian (Fig. 2). The climate in Abeokuta is classified as Aw based on the Koopen–Geiger (Essenwanger 2003) system. This implies a tropical region with a dry winter season and a wet summer season. There are two tropical local climate seasons prevalent in the study area. The long wet season runs from March–October while the dry season occurs from November–March when the area is under the influence of north-easterly winds (Badmus and Olatinsu 2010). The amount of rainfall in Abeokuta during the wet season varies between 750 and 1000 mm while it varies between 250 and 500 mm during the dry season (Akanni 1992). The mean monthly temperature ranges between 25.7 °C in July to 30.2 °C in February with a mean annual temperature of 26.6 °C. The relative humidity in Abeokuta varies from about 60–75% in months of November–March and about 80–90% in the month of April/October. Abeokuta is characterized by undulating topography with surface elevation ranging between 100 and 400 m above sea level (Akanni 1992; Oloruntola and Adeyemi 2014). The city of Abeokuta is drained by two major rivers, the Ogun and Oyan, and many small streams. Some of these small streams take their sources from local rocky hills while some are distributaries to the two major rivers (Adekunle et al. 2013). The investigated road portion is within the first 2 km of the roadway from the camp junction end where there were noticeable forms of surface depressions indicating failure on the road section.

Geology of the study area

The study area falls within the Basement Complex formation of southwestern Nigeria. Abeokuta is located on crystalline basement complex of igneous and metamorphic origin (Gbadebo et al. 2010). The basement rocks are of Precambrian age to early Paleozoic age and extend from the north-eastern part of Ogun state, of which Abeokuta belongs, and dipping towards the coast (Ako 1979). The basement complex rock comprises coarse–porphyritic hornblende–biotite–granodiorite, biotite granite gneiss, pegmatite, porphyroblastic granite gneiss, quartz–schist, and amphibolite/mica–schist (Jones and Hockey 1964; Kehinde-Phillips 1992). The foliation and joints on these rocks control the course of the two major rivers of Ogun and Oyan causing them to form a trellis pattern. The prolonged weathering of the crystalline rock has led to the development of regoliths of varying thicknesses which ultimately reduced the conductivity of the parent rocks (Badmus and Olatinsu 2010). The degree of weathering also depends on the depth of the rock beneath the earth surface. Abeokuta belongs to the stable plate which was not subjected to intense tectonics in the past; thus, the underground faulting system is



Fig. 1 Photo showing the state of the road. **a** Bad portion, **b** poor portion, **c** fair portion while **d** good portion of the road

minimal (Ufoegbune et al. 2009). Abeokuta is also said to be part of the transition zones of southwestern Nigeria. The northern side of Abeokuta is characterized by pegmatitic veins underlain by granite while the southern part enters the transition zone with the sedimentary formation of the

eastern Dahomey Basin. The western part of Abeokuta is characterized by granitic gneiss of a less porous nature together with various quartzite intrusions (Key 1992). At the southeastern and southwestern parts of the area is the outlier of the Ise formation of the Abeokuta Group which consists

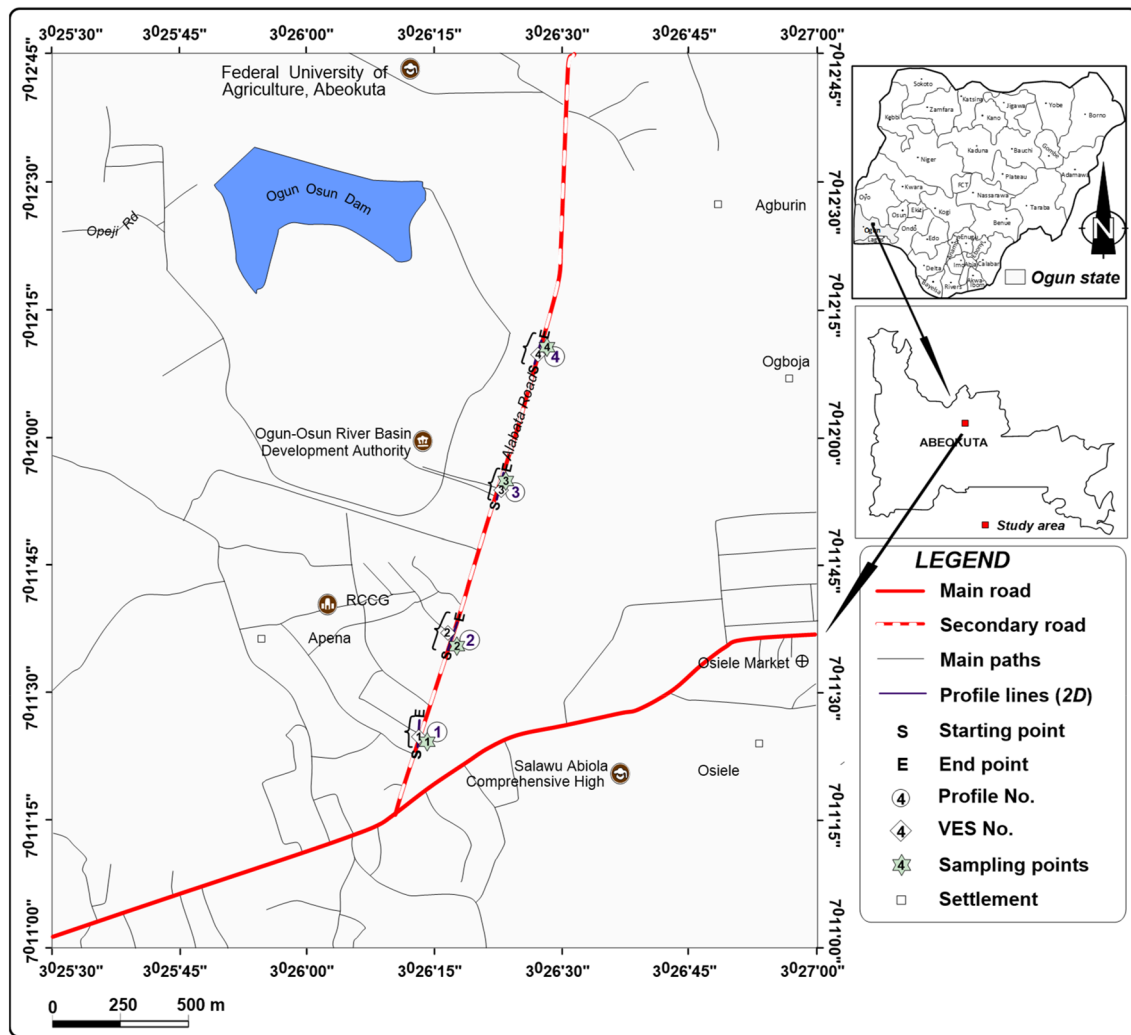


Fig. 2 Map showing location of the study area

of conglomerates and grits at the base that are overlain by a coarse medium grained loose sand (Aladejana and Talabi 2013). Outcrops of cross-bedded, ferruginous sandstones and pebbly sandstones have been noted near the base of the succession among the outliers south-east of Abeokuta (Jones and Hockey 1964). The terrain of Abeokuta is characterized by two types of landforms; these are sparsely distributed low hills and knolls of granite, other rocks of basement complex and nearly flat topography (Adekunle et al. 2013). The dominant rock type in the study area is migmatite gneiss as shown in Fig. 3

Methodology

In this research work, VES and 2D ERT surveys as well as soil laboratory analysis of some selected hydraulic properties were carried out. The VES and 2D ERT were used in this study because the two different applications of the

same electrical method can be used to study the geological structure of the subgrade layer of the pavement system. The 1D soundings allow the determination of the variation in the geoelectric parameters with depth at the probed points while the 2D ERT mapped resistivity continuity helpful to delineate structural weak/incompetent zones that could be responsible for incessant road failure. The investigated flexible pavement was divided into four sections based on the state/condition of the road at the time of the survey.

Resistivity data collection

Four traverses, each of length 100 m was established parallel to the road pavement along the designated four road sections for the 2D ERT survey in the S–N direction along the four designated road segments (Fig. 4). From the camp junction end of the road where there are noticeable forms of depressions, the road was designated into bad, poor,

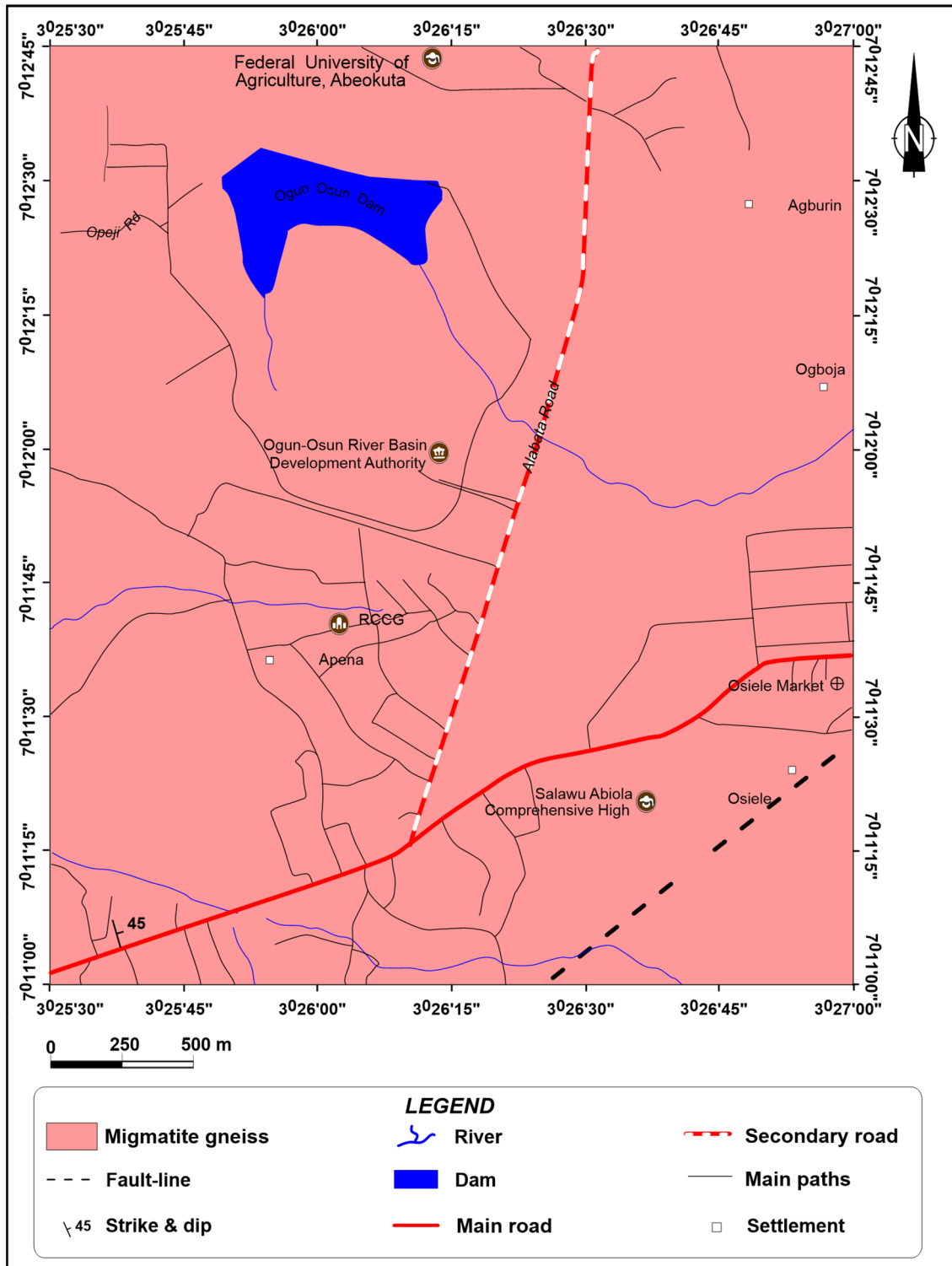


Fig. 3 Geological map showing the rock type that underlies the study area (modified after NGSa 2016)

fair, and good road sections. Traverse 1 was laid along the bad road section, traverse 2 was laid along the poor road section, traverse 3 was laid along the fair road section while traverse 4 was laid along the good road section.

Traverses 1 and 2 were considered failed road sections in this study. The electrode arrangement employed for the 2D ERT was the Wenner array with an electrode spacing ranging from $a = 3$ to $a = 12$ m at incremental step of 3

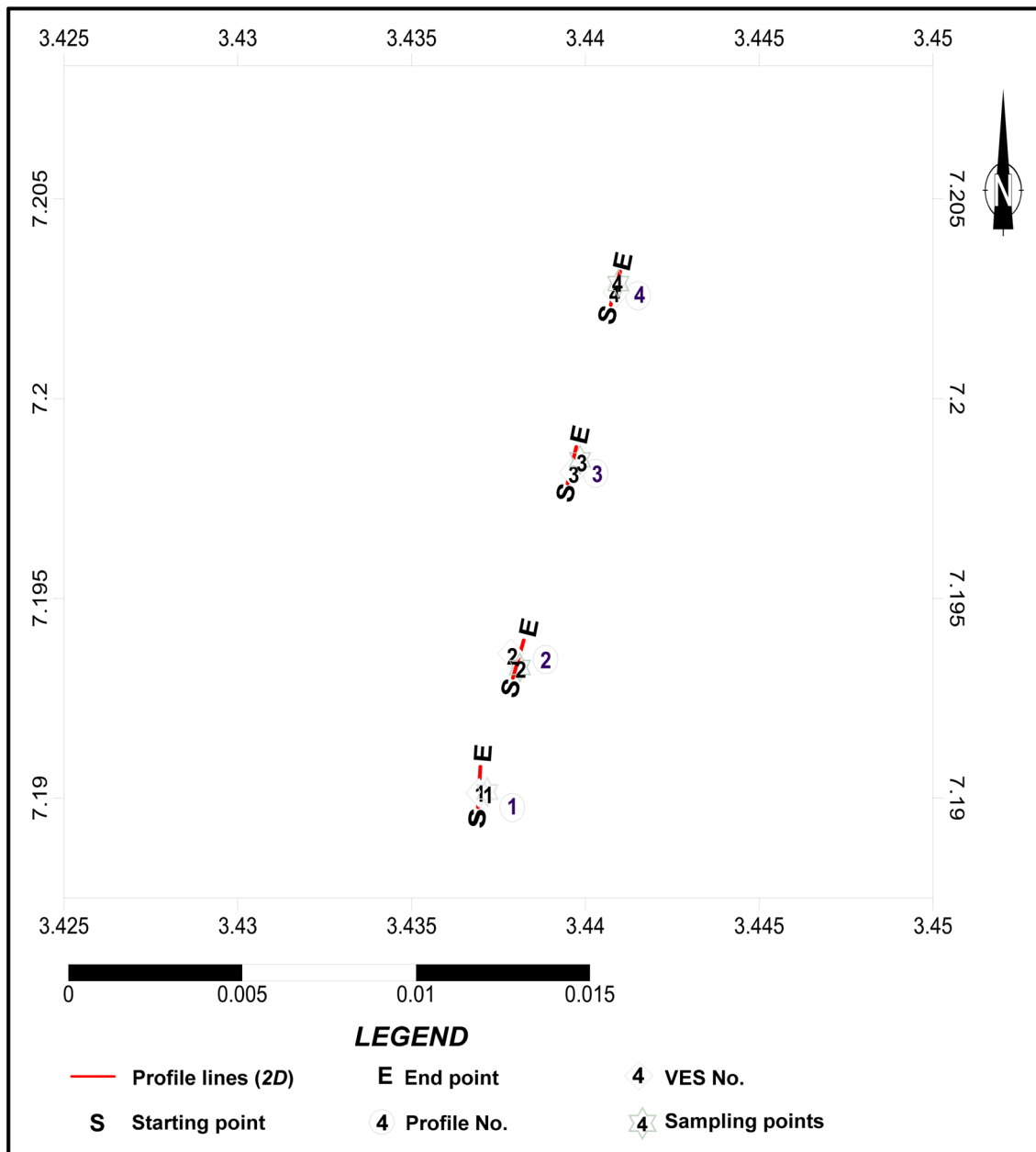


Fig. 4 Data acquisition map showing the 2D Traverse lines, VES points, and soil sampling points

across 100 m long traverse, resulting in four depth levels. The Wenner array was used for the 2D ERT because it gives high anomaly effect and a high signal to noise ratio (Danielsen and Dahlin 2009; Donohue et al. 2012). The equipment used for the measurement of resistivity data was Campus Omega (4-Channels) resistivity meter with serial no: 0086 manufactured by Allied Associates Geophysical Limited, United Kingdom. ERT data for each profile were acquired by means of a conventional Wenner survey with readings of each field resistance value using four electrodes with the resistivity meter. For the measurement,

the resistivity meter was set for four-cycle stacking and a standard error of measurements of less than 1%.

The 2D ERT raw data were processed and inverted with RES2DINV software (Loke and Barker 1996; Loke 2008). The software automatically determines the 2D resistivity model of the subsurface from the input 2D resistivity data using a smoothness-constrained least square method (Sasaki 1992; Devendran et al. 2003). The 2D model used by RES2DINV divides the subsurface into a number of rectangular blocks with resistivities that will produce an apparent resistivity section that agrees with the actual measurement.

The iterative optimization method tries to reduce the difference existing between the measured and calculated resistivity values with the inversion model. The accuracy of fit is expressed in terms of RMS error (Loke and Barker 1996; Loke et al. 2004).

A total of four VES were also carried out at each VES location chosen at the middle of the 2D traverse line (Fig. 4). The approximate distance between two successive VES points VES 1, 2, 3, and 4 was in the order of 420, 540, and 560 m, respectively. The electrode arrangement employed for each VES was a Schlumberger array with a maximum current electrode separation of 110 m. The VES resistivity data obtained in the field were partially curve matched before being computer iterated with WINResist software (ITC, Netherlands) to generate model curve and geoelectric layer parameters (Van der Velpen 1998, 2004; Oni and Olorunfemi 2016; Oladunjoye et al. 2017).

Soil sample collection

Soil samples were collected from selected points on each of the four designated road sections. Soil samples on bad (traverse 1), poor (traverse 2), fair (traverse 3), and good (traverse 4) road sections were coded A, B, C, and D, respectively. The sampling point on each traverse was chosen based on a spot where there was evidence of visual damage (especially on road sections comprising traverses 1, 2 and 3). Five (5) soil samples were collected on each traverse at sampling depths of 0–0.2 m, 0.2–0.4 m, 0.4–0.6 m, 0.6–0.8 m, and 0.8–1.0 m making a total of twenty samples on all the four road sections/traverses. The disturbed soil samples were collected with the aid of soil auger and suitably packed inside a polythene bag and labeled properly for easy identification. Cylindrical cores (5 cm diameter and 5 cm in height) were also used to take undisturbed soil samples at varying depths for determination of saturated hydraulic conductivity, bulk density, and moisture content. The collected soil samples were analyzed in the soil physics laboratory of the Institute of Agricultural Research & Training (IAR&T), Moor Plantation, Ibadan, Nigeria. Soil parameters analyzed include particle size distribution, bulk density (BD), saturated hydraulic conductivity (K_{sat}), soil resistivity, Atterberg limit, and penetration resistance (PR). The particle size distribution was done according to the procedure outlined by Gee and Or (2002) with the help of the modified Bouyoucos hydrometer method. The textural classification was done using the USDA textural soil classification system. Soil moisture content was determined by the weight loss method based on the ASTM D4959-07 standard (ASTM D4959-07 2007). Soil resistivity was measured using the MC Miller soil boxes according to the ASTM G57-05 (ASTM G57-05 2005) standard. K_{sat} was measured using the constant head parameter method based on Reynolds and Elrick (2002).

The BD was determined by gravimetric soil core method as described by Grossman and Reinsch (2002) with the particle density assumed to be 2650 kg/m³. The porosity in (%) was calculated from the BD using the equation as described by Hillel (2004) where

$$\text{Porosity} = 1 - \frac{\rho_{bulk}}{\rho_{particle}} \quad (1)$$

where ρ_{bulk} = bulk density in g/cm³ and $\rho_{particle}$ = 2.65 g/cm³.

Atterberg's limit tests [plastic limit (PL), liquid limit (LL), and Plasticity index (PI)] were determined according to the ASTM D4318-10EI (ASTM D4318, 2017) standard. The PR of the soil was determined in situ using the electronic penetrometer developed by Eijkkamp Agrisearch Equipment, Netherland. Descriptive statistics and Analysis of variance (ANOVA) were performed on the soil data in order to determine if the selected soil parameters varied significantly among the four designated road sections.

The resistivity curves of VES and 2D ERT image sections together with the results of the soil analysis were integrated and correlated to assess the causes of incessant pavement failure along the investigated road.

Results and discussions

The summary of the interpreted VES result is shown in Table 1 while the results obtained from the VES are shown in Fig. 5. The dominant curve type obtained for this study is H-type. The analysis and interpretation of the VES curves and obtained geoelectric parameters indicated that three layers were delineated. These are topsoil, clayey weathered layer, and fractured/fresh basement. The topsoil resistivity values range from 71 to 282 Ω m with a mean value of 167 Ω m, and thickness values range from 0.9 to 3.2 m with mean value of 2.3 m. The topsoil resistivity values for VES 3 and 4 (under fair and good road sections) are greater than 200 Ω m while low resistivity values (< 200 Ω m) were obtained for topsoil at VES 1 and 2 (failed road sections). From the VES results, the topsoil of VES 1 and 2 have relatively low resistivity values (110 and 71 Ω m). This is an indication of incompetent weak topsoil characterized by clay and sandy clay materials with strong affinity for water, thus unsuitable as subgrade layers for stable pavement, hence the state of road sections under VES 1 and 4. The clayey weathered layer has resistivity values ranging from 12 to 76 Ω m with mean value of 41 Ω m and thickness values ranging from 7.1 to 22 m with a mean value of 16 m. The low resistivity value (< 100 Ω m) for this layer is an indication of clay soil at all the VES points. The low resistivity clay soil implied that this layer is geotechnically incompetent to withstand engineering structures such as pavement (Egwuonwu

Table 1 Summary of the geoelectric parameters from VES inversions

Station	Layers no	Resistivity (Ωm)	Thickness (m)	Depth (m)	Curve type	Probable lithology
VES 1	1	110	2.6	2.6	H	Topsoil
	2	12	4.5	7.1		Weathered basement (Clayey)
	3	10,094	–	–		Fresh basement
VES 2	1	71	0.9	0.9	KH	Top soil
	2	142	1.9	2.8		Clayey sand
	3	26	6.2	9.0		Weathered basement (Clayey)
	4	336	–	–		Fractured basement
VES 3	1	207	2.6	2.6	H	Topsoil
	2	36	17.2	19.8		Weathered basement (Clayey)
	3	261	–	–		Fractured basement
VES 4	1	282	3.2	3.2	H	Topsoil
	2	76	19.1	22.3		Weathered basement (Clayey)
	3	1203	–	–		Fresh basement

and Osazuwa 2011; Oladunjoye et al. 2017). Similarly, clay/sandy clay response to vehicular load and swellings causes differential stress on the pavement. The last layer is the fractured/fresh basement with resistivity values ranging from 234 to 10,094 Ωm with mean value of 2948 Ωm . VES 2 and 3 have resistivity values less than 500 Ωm while VES 1 and 4 have resistivity values of the bedrock > 1000 Ωm .

Interpretation of 2D resistivity model

The inverse model sections of the 2D ERT are presented in Fig. 6. Figure 6a shows model section for traverse 1 with RMS error of 2.4%. This traverse was laid parallel to the failed part of the road section. The model of this traverse shows the surface and near-surface layers are characterized by resistivity values ranging from 69 to 131 Ωm with a thickness of less than 4 m. This is an indication of shallow geotechnically incompetent materials. This corresponds with a topsoil layer of VES1 (clayey sand) with a resistivity of 110 Ωm at a depth of 2.6 m. Intensely weathered rocks of high moisture content (<30 Ωm) occurring at different depths along lateral distance of 0–60 m of the traverse may have aided differential settlement of subgrade and consequent failure of the road (Adabanija et al., 2016; Adiat et al., 2017). vertical linear geologic structure, mainly due to differential weathering was noticed at lateral distance 66–82 m in the northern side of the traverse. A resistive region with resistivity values ranging from 181 to 251 Ωm were observed at lateral distance 87–92 m of the traverse which was debris of asphalt piles on the road section during the field work. The inversion model of traverse 2 (Fig. 6b) established on another failed section of the road depicts a resistivity distribution that varied from 36 to 131 Ωm . The RMS error for the pseudosection for traverse 2 was 3.9%. The 2D section was unable to depict the fractured basement

as captured by the model from VES 2. The model of the 2D section shows that there is presence of weathered materials of relatively low resistivity value (69–95 Ωm) that extends from the surface downward at lateral distance 5–15 m of the traverse.

The resistivity depth model of traverse 2 as shown in Fig. 6b shows topsoil resistivity values in the range of 50–131 Ωm . This resistivity range (50–131 Ωm) falls within incompetent topsoil (Oladapo et al. 2008; Adabanija et al. 2016) with a shallow depth of about 2.0 m. However, The 1D model of VES 2 showed top soil with resistivity value of 71 Ωm at a depth of 0.9 m. An intrusion of weathered materials of resistivity values (70–95 Ωm) protrudes to the surface at lateral distances of 4–16, 43–51, 60–75, and 78–95 m along the traverse. A low resistive (conductive zone) region with the resistivity values ranging from 26–50 Ωm were seen from lateral distance of 27 m to the end of the traverse. This is an indication of extensive saturated zone with high moisture content, hence one of the likely causes of the poor state of the road section. This corresponds with weathered (clayey) layer of VES 2 result with resistivity value of 25 Ωm . The 2D model section of traverse 2 showed very thin (from not present up to 1.25 m thick) topsoil and is not spread across the whole length of the traverse. The 2D model section of this traverse did not show fractured basement as depicted by 1D model of VES 2. Figure 6c shows the inverted section (with RMS error of 4.5%) of traverse 3 which lies along the S–N direction of fair portion of the road section. The 2D model shows that its topsoil was marked by a resistivity distribution ranging from 69 to 181 Ωm . This is an indication of clayey sand topsoil with varying depths. The 1D model for VES 3 indicates topsoil with resistivity value of 207 Ωm at a depth of 2.6 m. Below the topsoil is a weathered basement layer (clay rich soil) with resistivity values > 20 $\Omega\text{-m}$ and < 50 $\Omega\text{-m}$ of nearly the same depth at

Fig. 5 **a, b** Layer Model Interpretations for VES 1 and VES 2. **c, d** Layer Model Interpretations for VES 3 and VES 4

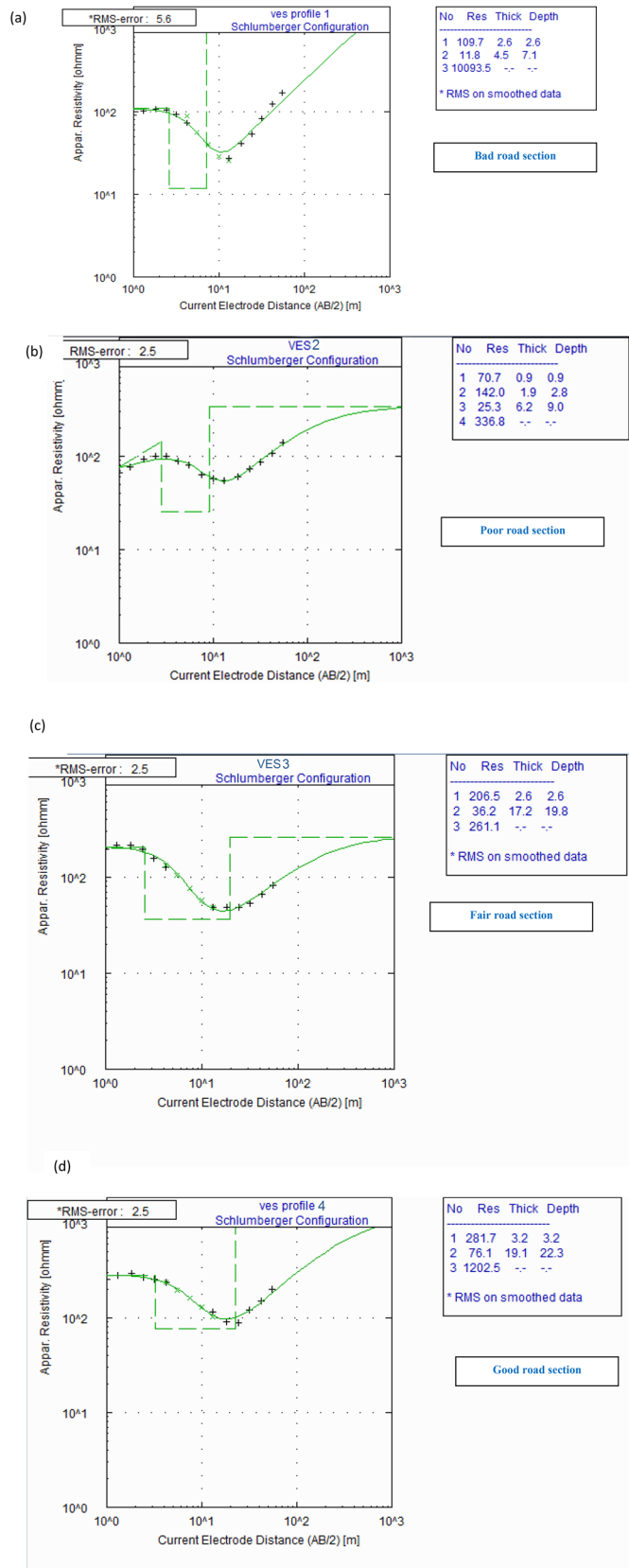
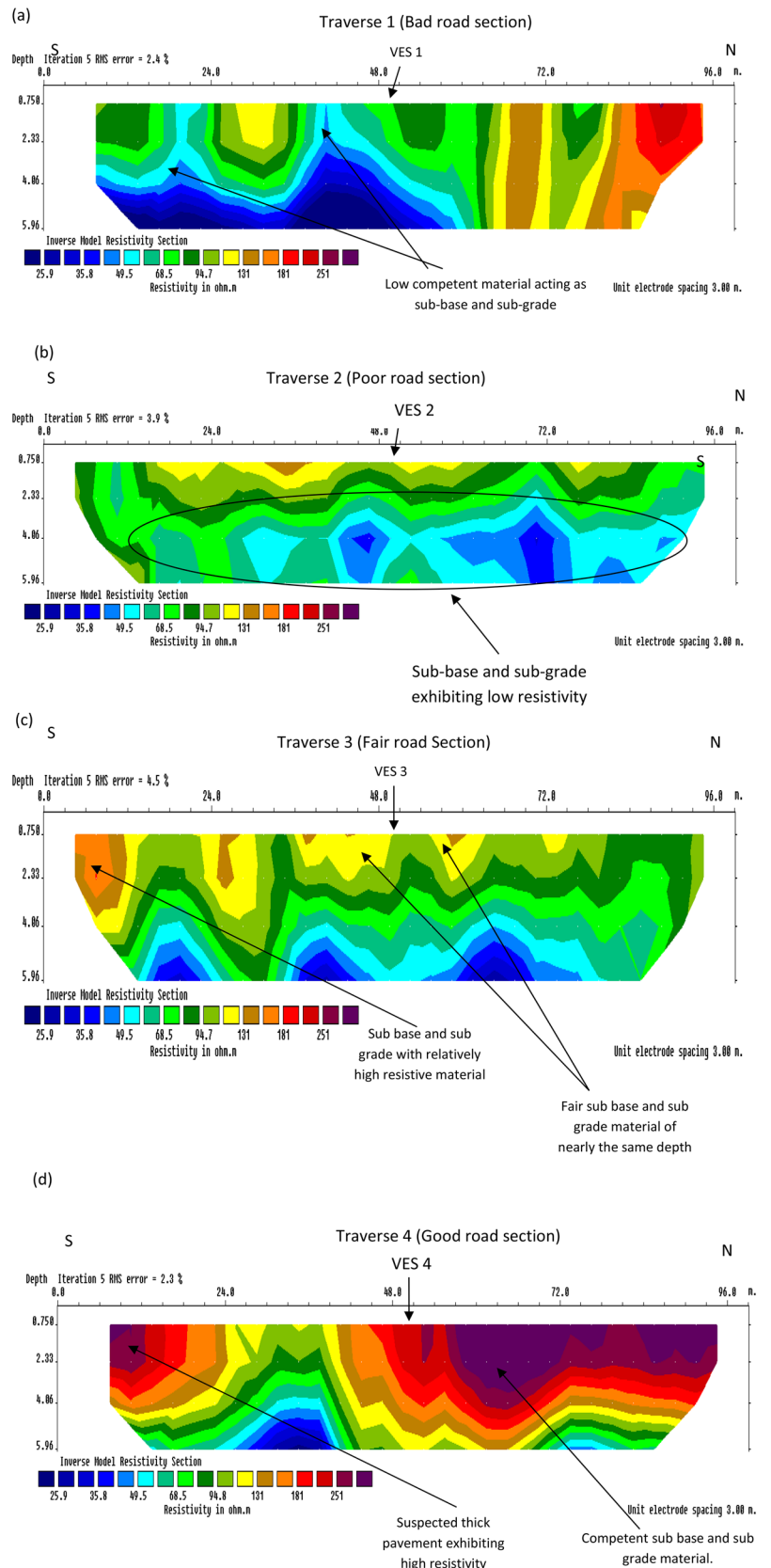


Fig. 6 a–d 2D inverse resistivity model for traverses 1, 2, 3, and 4



lateral distances of 15–24 and 36–80 m along the traverse. This is an indication of clayey soil. The weathered layer in the 2D model of this traverse corresponds with clay having resistivity of 36 Ωm below the topsoil of VES 3. The fair stability of the pavement along this traverse maybe due to subgrade of nearly the same depth, which can thus reduce differential settlement of subbase and subgrade which could have led to the failure of the road pavement. However, a 2D model of traverse 3 was unable to show fractured basement as depicted by VES model interpretation.

Figure 6d shows model section for traverse 4 (RMS error 2.3%) which was laid parallel to the good section of the road. The resistivity depth model shows relatively high resistivity value (181–251 Ωm) for the topsoil which is extensive at lateral distances 7–24 m and from 40 m up to the end of the traverse with a depth of about 4 m. High resistivity value of the topsoil is an indication of competent topsoil with low moisture content and absence of clay, this topsoil typically sustains the pavement on this road section. From the VES 4 result, relatively thick clayey sand material constitutes the top soil of the good road section. The 1D model obtained from VES 4 indicates topsoil with a resistivity of 282 Ωm at a depth of 3.2 m. The second layers (clay rich layer) of 2D section was characterized with resistivity values less than 60 Ωm and were observed at lateral distance of 27–39 and 72–75 m along the traverse at depths of 4.1–5.9 and 5.7–5.9 m, respectively. This weathered layer corresponds with a layer below the topsoil of VES 4 with a resistivity of 76 Ωm which is clayey in nature. There is presence of an anomaly with high resistivity value ($> 251 \Omega\text{m}$) at lateral distance 44–100 m of the traverse from the surface up to a depth of 4 m, an indication of competent subbase and subgrade material underlying the thick pavement and thus acting as a support. The third layer was not imaged by the 2D inverse model because it occurs at a greater depth of about 22 m as shown by VES 4 result. There is lateral discontinuity/intrusive between lateral distance 24 and 40 m along this traverse.

The maximum depth of penetration obtained for the 2D ERT section was 5.9 m while the maximum depth of penetration by VES model was 22 m. Comparison between the VES results and 2D imaging sections showed that there is similarity in thicknesses and resistivity values for some geoelectric layers. The combined results of VES and 2D ERT attributed failure on road sections (traverses 1 and 2; VES 1 and 2) to incompetent topsoil with resistivity values less than 200 Ωm . Low resistivity clay enriched the weathered layer at shallow depth and differential settlement was induced by the clayey substratum. This result concurs with earlier, similar results obtained by Momoh et al. (2008); Oladapo et al. (2008); Akintorinwa, et al. (2011) which reported resistivity values of $< 200 \Omega\text{m}$ for topsoil and shallow depth of weathered layer for studied failed road segments.

Result of soil analysis

The result of soil analyses on selected hydraulic and geotechnical properties are presented in Table 2 while Table 3 shows the mean values of analyzed parameters on the investigated four road sections. Table 4 shows the ANOVA result while Table 5 shows the details of the descriptive statistics of the analyzed hydraulic and geotechnical properties from the four road sections. The soil analyses are for samples collected from depths of 0–100 cm (i.e. the topsoil with thickness values ranging from 0.9 to 3.2 m with mean value of 2.3 m). The mean percent content of sand, silt, and clay in all the samples ranged from 64.9 to 73.2%; 9.7–16.3% and 16.9–18.7%, respectively. The mean % sand content is highest in soil samples collected on the good road section (traverse 4) while the lowest % sand content was found in samples on one of the failed road sections (traverse 1). The highest mean % silt value (16.3) occurred in bad road section (traverse 1) samples while analyzed soil samples on traverse 4 have the least value of % silt content (9.66). This result buttressed earlier reported negative correlation between particle size distributions of sand and silt in experimental tropical soil (Shukla et al. 2006; Ayoubi et al. 2011). However, the highest and lowest mean % clay content (18.7 and 16.9, respectively) were obtained for soil samples on traverses 1 and 2 (failed road sections). Soil textural classes for samples collected between 0.6 and 1.0 m depth in both failed road sections (traverses 1 and 2) belong to sandy clay loam while there is uniformity in soil textural class for soil samples on traverse 4 at each sampling depth. The mean soil moisture content (MC) on all analyzed soil samples ranged from 8.9 to 9.8%. The highest mean MC was obtained for samples on traverse 1 (failed road section) compared to least value of average MC (8.9) in soil samples of traverse 4 (good road section). The relatively highest mean MC value obtained for samples on traverse 1 may be due to its relatively highest mean % clay content (18.7). However, all the analyzed soil samples have MC below 10% at the time of study and can be rated as fair to poor subgrade foundation materials (Okpoli 2014). The mean Bulk Density (BD) and porosity range from 1.50 to 1.53 Mg/m^3 and 42.1–43.3%, respectively. However, the differences in BD and porosity were not significant at 5% level (as shown in Table 4). The bad and good road sections (on traverses 1 and 4) have the same numerical value of mean BD while the fair road section had least value of mean BD. The highest average Bulk Density value (1.53 Mg/m^3) was noticed in soil samples collected on traverse 2 (another failed road section) with corresponding least mean porosity value. This result confirmed the inverse relationship between BD and porosity of experimental soil samples (Vogelmann et al. 2010).

Table 2 Results of particle size analysis and geotechnical analysis

Description	Sand (%)	Clay	Silt	Textural class	Bulk density (Mg/m ³)	Porosity (%)	MC (cm ³ /cm)	SHC (cm/h)	Soil resistivity (Ω cm)	Atterberg limit		Penetration resistance (MPa)
										LL (%)	PL	
A												
0–20 cm	65.76	12.22	22.02	SL	1.55	41.5	0.106	1.90	6.21	24.32	17.59	113.86
20–40 cm	64.46	16.35	19.19	SL	1.52	42.6	0.097	0.89	4.64	21.43	17.25	80.09
40–60 cm	66.46	19.36	14.18	SL	1.50	43.4	0.097	0.60	3.92	25.04	17.02	63.10
60–80 cm	63.24	23.36	13.40	SCL	1.48	44.2	0.096	0.32	3.25	29.81	16.79	49.56
80–100 cm	64.72	22.38	12.90	SCL	1.49	43.8	0.096	0.36	3.39	28.75	16.91	55.95
B												
0–20 cm	76.38	11.42	12.2	SL	1.59	40.0	0.098	2.20	6.65	15.66	18.04	180.12
20–40 cm	72.36	14.35	13.29	SL	1.57	40.8	0.097	1.09	5.29	19.43	17.81	143.42
40–60 cm	67.34	17.34	15.32	SL	1.53	42.3	0.095	0.66	4.38	22.88	17.36	90.13
60–80 cm	64.56	20.54	14.90	SCL	1.50	43.4	0.097	0.40	3.70	26.57	17.02	63.10
80–100 cm	64.35	21.04	14.61	SCL	1.48	44.2	0.098	0.50	3.61	26.85	16.79	49.56
C												
0–20 cm	72.12	13.44	14.44	SL	1.53	42.3	0.092	2.08	5.65	17.73	17.36	90.13
20–40 cm	71.42	15.23	13.35	SL	1.53	42.3	0.096	1.18	4.99	20.09	17.36	90.13
40–60 cm	68.42	18.45	13.13	SL	1.51	43.0	0.093	0.71	4.12	24.02	17.13	71.12
60–80 cm	68.12	19.56	12.32	SL	1.48	44.2	0.095	0.64	3.88	24.96	16.79	49.56
80–100 cm	67.14	22.34	10.52	SCL	1.46	44.9	0.097	0.51	3.40	28.12	16.56	38.79
D												
0–20 cm	78.19	13.84	7.97	SL	1.51	43.0	0.091	2.53	5.49	18.02	17.13	71.12
20–40 cm	75.19	14.34	10.47	SL	1.52	42.6	0.097	1.75	5.30	18.79	17.25	80.09
40–60 cm	72.87	18.56	8.57	SL	1.50	43.4	0.084	0.71	4.09	24.00	17.02	63.10
60–80 cm	72.55	18.72	8.73	SL	1.51	43.0	0.083	0.64	4.06	24.37	17.13	71.12
80–100 cm	67.34	20.12	12.54	SL	1.49	43.8	0.094	0.58	3.77	25.85	16.91	55.95

A soil samples on traverse 1, B soil samples on traverse 2, C soil samples on traverse 3, D soil sample on traverse 4, SL sandy loam, SCL sandy clay loam, MC moisture content, SHC saturated hydraulic conductivity, LL liquid limit, PL plastic limit, PI plastic index

Table 3 Mean values of analyzed soil properties

Location of soil samples	Clay %	Silt %	Sand %	Mean porosity (%)	Mean BD (Mg/m ³)	Mean K _{sat} (cm/h)	MC cm ³ /cm ³	Soil resistivity (Ω cm)	PL	LL	PI	Penetration resistance (MPa)
Bad road section (BRS)	18.7	16.34	64.9	43.1	1.51	0.81	0.0984	4.28	17.11	25.87	8.76	72.51
Poor road section (PRS)	16.9	14.06	68.9	42.1	1.53	0.97	0.0970	4.72	17.40	22.28	5.82	105.27
Fair road section (FRS)	17.8	12.75	69.4	43.3	1.50	1.02	0.0950	4.41	17.04	22.98	5.94	67.94
Good road section (GRS)	17.1	9.66	73.2	43.2	1.51	1.24	0.0898	4.54	17.08	22.21	5.12	68.27

The Atterberg's limits results showed that the mean Liquid Limit (LL), Plastic Limit (PL), and Plasticity Index (PI) in % ranged from 22.2 to 25.9; 17.04–17.40 and 5.12–8.76, respectively. A close observation of PI and LL average values shows that highest mean PI and LL values (8.76 and 25.87) were found in soil samples of traverse1(failed section) while lowest mean PI and LL values (5.12 and 22.21) were found in soil samples collected on traverse 4 and can be classified as competent nonexpansive subgrade. The PI value increases with sampling depths for both the fair (traverse 3) and good road sections (traverse 4) but with no clear trends for samples on traverses 1 and 2 (failed road sections). The < 10% PI value for sampling depth 0 – 40 cm (regarded as subgrade layer based on the Ohio Department of Transportation (Igwe et al. 2013) specification) on traverse 4 samples indicates that the topsoil is very weak in retaining water (Igwe et al. 2013). However, the mean value of PL, LL and PI lies within the recommended limits for tropical road by FMWH (2000). The range of mean saturated hydraulic conductivity (K_{sat}) for analyzed samples in all investigated road sections ranged from 0.81 to 1.24 cm/h. The relatively highest mean K_{sat} value was obtained at traverse 4 (GRS) while samples on traverse 1(failed section) had the lowest mean K_{sat} value (0.81 cm/h). The highest value of K_{sat} on traverse 4 buttressed its stable state and corroborates its lowest mean PI value.

The average soil resistivity value ranged from 4.28 to 4.72 Ω cm. The highest mean soil resistivity was found in traverse 2 soil samples while lowest mean soil resistivity was found in traverse1 samples. Soil sample at depth of 60–80 cm in traverse1 had lowest value of soil resistivity (3.25 Ω cm) with relatively highest clay content (23.36%) and highest PI value (13.02%) among all the analyzed soil samples. This may be due to the fact that clay content facilitates surface conductance of electrical current (Long et al. 2012). The result was also in agreement with an earlier result of Long et al. (2012) who reported a trend of decreased resistivity with increased clay content and PI. However, soil resistivity value in each sampling depth for all the investigated road sections lies below 10 Ω-cm. There is no clear trend of variation of soil resistivity values with moisture content and BD. This may be due to limited range of values studied (Long et al. 2012).

The in situ Penetration Resistance (PR) values for each sampling depth in all the investigated road section ranged from 38.78 to 180.12 MPa (Table 2). The mean PR value for analyzed soil samples ranged from 67.9 to 105.3 MPa (Table 3). The highest mean PR value was found in soil samples of traverse 2 (PRS), followed by that of traverse 1 (BRS) while the mean PR of samples on traverses 3 and 4 (FRS and GRS) were nearly the same (though, lowest mean PR was found in traverse 3 soil samples). The trend of variation of mean PR values among the investigated road

Table 4 ANOVA results for analyzed parameters based on the road sections

Parameters	Bad	Poor	Fair	Good
% Sand	64.93 ± 1.24 ^a	69.00 ± 5.24 ^{ab}	69.44 ± 2.19 ^{ab}	73.23 ± 3.99 ^b
% Clay	18.73 ± 4.56 ^a	16.94 ± 4.09 ^a	17.80 ± 3.53 ^a	17.12 ± 2.83 ^a
% Silt	16.34 ± 4.05 ^a	14.06 ± 1.29 ^{ab}	12.75 ± 1.46 ^{bc}	9.66 ± 1.86 ^c
BD	1.51 ± 0.03 ^a	1.53 ± 0.05 ^a	1.50 ± 0.03 ^a	1.51 ± 0.01 ^a
Porosity	43.10 ± 1.07 ^a	42.14 ± 1.75 ^a	43.34 ± 1.17 ^a	43.16 ± 0.46 ^a
MC	0.0984 ± 0.00 ^a	0.0970 ± 0.00 ^a	0.0946 ± 0.00 ^{ab}	0.0898 ± 0.00 ^b
SHC	0.81 ± 0.65 ^a	0.97 ± 0.74 ^a	1.02 ± 0.64 ^a	1.24 ± 0.87 ^a
Soil resistivity	4.28 ± 1.21 ^a	4.73 ± 1.27 ^a	4.41 ± 0.90 ^a	4.54 ± 0.79 ^a
LL	25.87 ± 3.41 ^a	22.28 ± 4.79 ^a	22.98 ± 4.10 ^a	22.21 ± 3.55 ^a
PL	17.11 ± 0.32 ^a	17.40 ± 0.52 ^a	17.04 ± 0.36 ^a	17.09 ± 0.13 ^a
PI	8.76 ± 3.65 ^a	5.82 ± 4.30 ^a	5.94 ± 4.43 ^a	5.12 ± 3.65 ^a
Penetration resistance	72.51 ± 25.77 ^a	105.27 ± 55.16 ^a	67.95 ± 23.36 ^a	68.28 ± 9.14 ^a

The table shows mean ± SD. Values along the same row with different superscripts are significantly different at 5% ($p < 0.05$)

sections buttressed the inverse relation between porosity and PR. For instance, lowest mean porosity (42.1%) was found in soils of PRS (with the corresponding highest mean PR), followed by that of BRS, while soil samples on traverses 3 and 4 had nearly the same numerical value of mean porosity. Compaction of subgrade layer may have occurred on PRS as shown by the lowest mean porosity (42.1%), lower mean K_{sat} (0.97 cm/h), highest mean BD (1.53 Mg/m³), and highest mean PR (105.27 MPa). This is corroborated by very thin to no topsoil along the traverse as shown by the 2D ERT section of traverse 2 (i.e. Fig. 6b), hence lower aggregate stability of the topsoil on traverse 2 and sensitivity to surface crusting (Cook et al. 1986). Moreover, the highest mean values of PR and BD of subgrade soil samples on PRS imply impeded drainage could be encountered through this layer (Materechera 2018). However, based on the Ohio Department of Transportation (ODOT 2002) specification boundary depth for subgrade layer (0–300 mm), the PR value increases within this depth range (0–20 and 20–40 cm) for soil samples D on traverse 4 (stable portion) but with no clear trend at other sampling depths. On traverse 3 (soil samples C, fair section), the PR shows no change at depths 0–20 and 20–40 cm but shows a steady decrease from sampling depth range 40–60 cm up to 80–100 cm. On traverse 1 (soil samples A), the PR value decreases from 113.86 MPa at sampling depth 0–20 cm to 80.09 MPa at depth 20–40 cm. However, traverse 1 shows an increase in PR at the bottom zone (soil depth 80–100 cm). For traverse 2 (soil samples B), the PR value also decreases from 180.12 to 143.42 MPa within the ODOT depth range (0–20 cm and 20–40 cm) but shows steady decrease from sampling depth 40–60 cm to 80–100 cm. The result of increases in PR within the ODOT subgrade depth obtained for samples on traverse 4 agrees with the earlier reported fact that the maximum PR allowed while still sustaining the vertical stress induced by surface

loading on the subgrade layer increases as depth increases (Wu and Sargand 2007). The BD value decreases with sampling depths on both bad and poor road sections (soil samples A and B). Specifically, the soil BD decreases with ODOT subgrade layer depth in both BRS and PRS. The BD on traverse 3 (fair road section, soil samples C) shows no change from 0–20 to 20–40 cm but shows slight decrease from sampling depth 40–60 cm to 80–100 cm. However, BD increased slightly within ODOT subgrade layer depth in good road section (traverse 4, soil samples D) but with no clear trend of variation at other sampling depths. This result further buttressed the direct relationship between Bulk Density and Penetration Resistance; hence PR can be used as an indicator of soil compaction status (Vanags et al. 2004). From Table 4, the differences in percent clay, porosity, BD, K_{sat} , soil resistivity, LL, PL, PI, and PR in all the analyzed soil samples were not significant among the different road sections at a 5% level while there were significant differences in values of % sand, % silt, and MC at a 5% level ($p < 0.05$) among the four different road sections. The ANOVA result further shows that % sand for the bad road section differs significantly from the % sand for the good road section. The % silt and MC vary significantly among the different sections of the road.

Conclusions

An integrated investigation involving electrical resistivity surveys (VES and 2D ERT) and soil analyses were performed on flexible pavement to effectively characterize the subsoil upon which the pavement has been laid. The heterogeneous nature of the subsurface layer emphasized the need for combined geoelectrical and soil analysis to effectively study causes of unceasing failures on Camp–Alabata road.

Table 5 Descriptive statistics of analyzed soil parameters based on the road sections

Parameters	Category	Mean	SD	SE	CV (%)
% Sand	Bad	64.93	1.24	0.55	1.9
	Poor	69.00	5.24	2.34	7.6
	Fair	69.44	2.19	0.98	3.2
	Good	73.23	3.99	1.79	5.5
% Clay	Bad	18.73	4.56	2.04	24.3
	Poor	16.94	4.09	1.83	24.2
	Fair	17.80	3.53	1.58	19.8
	Good	17.12	2.83	1.27	16.6
% Silt	Bad	16.34	4.05	1.81	24.8
	Poor	14.06	1.28	0.58	9.2
	Fair	12.75	1.46	0.65	11.4
	Good	9.66	1.86	0.83	19.3
BD	Bad	1.51	0.03	0.01	1.8
	Poor	1.53	0.05	0.02	3.0
	Fair	1.50	0.03	0.01	2.1
	Good	1.51	0.01	0.00	0.8
Porosity	Bad	43.10	1.07	0.48	2.5
	Poor	42.14	1.75	0.78	4.1
	Fair	43.34	1.17	0.52	2.7
	Good	43.16	0.46	0.20	1.1
MC	Bad	0.10	0.00	0.00	4.3
	Poor	0.10	0.00	0.00	1.3
	Fair	0.09	0.00	0.00	2.2
	Good	0.09	0.00	0.00	6.8
SHC	Bad	0.81	0.65	0.29	79.6
	Poor	0.97	0.74	0.33	75.9
	Fair	1.02	0.64	0.29	62.7
	Good	1.24	0.87	0.39	69.7
Soil resist	Bad	4.28	1.21	0.54	28.2
	Poor	4.73	1.27	0.57	26.8
	Fair	4.41	0.90	0.40	20.5
	Good	4.54	0.79	0.35	17.4
LL	Bad	25.87	3.41	1.53	13.2
	Poor	22.28	4.79	2.14	21.5
	Fair	22.98	4.10	1.83	17.9
	Good	22.21	3.55	1.59	16.0
PL	Bad	17.11	0.32	0.14	1.8
	Poor	17.40	0.52	0.23	3.0
	Fair	17.04	0.36	0.16	2.1
	Good	17.09	0.13	0.06	0.8
PI	Bad	8.76	3.65	1.63	41.7
	Poor	5.82	5.30	2.37	108.8
	Fair	5.94	4.44	1.99	74.7
	Good	5.12	3.65	1.63	71.2
Penetration resistance	Bad	72.51	25.77	11.53	35.5
	Poor	105.27	55.16	24.67	52.4
	Fair	67.95	23.36	10.45	34.4
	Good	68.28	9.14	4.09	13.4

Geoelectrical results showed that causes of failed sections (on traverses 1 and 2) can be attributed to low resistivity ($< 200 \Omega\text{m}$) topsoil, a clay-enriched shallow weathered layer, and differential settlement of subgrade materials with high moisture content. The stable section of the road was characterized by relatively thick topsoil/subgrade with high resistivity values ($> 200 \Omega\text{m}$), a thick weathered layer with resistivity values > 50 and $< 100 \Omega\text{m}$ and was generally devoid of differential settlement. The results of 2D ERT can be used to complement the results of VES. However, a 2D model section provides better resolution of spatial variation of resistivity, lithology, and structural features. Subgrade soils below stable pavement with resistivity values $> 200 \Omega\text{m}$ exhibited relatively lowest mean values of PI, MC, and % silt than their counterparts below failed sections. The analyzed soil samples from the stable good road section (traverse 4) have uniform soil textural class at all sampling depths, highest mean K_{sat} value, and an in situ PR value that increased with ODOT subgrade layer depth (0–20 and 20–40 cm). The PR value decreases with ODOT subgrade layer depth for the two failed road sections (traverses 1 and 2). An one-way ANOVA revealed that % silt and MC varied significantly at a 5% level for soils of different sections of the road. The ANOVA result further shows that the mean % sand content for the bad road section differs significantly from the mean % sand for the good road section. The Atterberg's Limit results showed that subgrade materials in the investigated road sections belong to fair to good engineering materials. Adequate engineering construction approaches should be adopted considering the thick layer of incompetent formation (clay) observed across the area investigated. A proper drainage system should also be established beside the roadway. The integrated use of geoelectrical and soil analysis allows for a better and more detailed understanding of the subsoil lithologies that have influence on the design of flexible pavement.

Compliance with ethical standards

Conflict of interest The authors declare that there is no conflict of interest.

References

- Abdullah W, AlJarallah R, AlRashidi A (2014) Hydrocarbon oil-contaminated soil assessment using electrical resistivity topography. *J Eng Res* 2(3):67–85. <https://doi.org/10.7603/s40632-014-0014-z>
- Adabanija MA, Adetona EA, Akinyemi AO (2016) Integrated approach for pavement deterioration assessments in a low latitude crystalline basement of south-western Nigeria. *Environ Earth Sci* 75:289. <https://doi.org/10.1007/s12665-015-5030-2>

- Adebisi NO, Ariyo SO, Sotikare PB (2016) Electrical resistivity and geotechnical assessment of sub-grade soils in southwestern part of Nigeria. *J Afr Earth Sci* 119:256–263
- Adekunle AA, Badejo AO, Oyerinde AO (2013) Pollution studies on groundwater contamination: water quality of Abeokuta, Ogun state, southwest Nigeria. *J Environ Earth Sci* 3(5):161–166
- Adeleye AO (2005) Geotechnical investigation of subgrade soil along sections of Ibadan-Ife Highway. Unpublished M.Sc Project, Obafemi Awolowo University, Ile-Ife, 181 pp
- Adesola AM, Ayokunle AA, Adebowale AO (2017) Integrated geophysical investigation for pavement failure along a dual carriage, Southwestern Nigeria: a case study. *Kuwait J Sci* 44(4):135–149
- Adeyemo JA, Omosuyi GO (2012) Geophysical investigation of Road pavement instability along part of Akure–Owo expressway, southwestern Nigeria. *Am J Sci Ind Res* 3(4):191–197
- Adiat KAN, Akinlalu AA, Adegoroye AA (2017) Evaluation of road failure vulnerability section through integrated geophysical and geotechnical studies. *NRIAG J Astron Geophys* 6:244–255
- Ajayi LA (1987) Thought on road failure in Nigeria. *Nig Eng* 22(1):10–17
- Akanni CO (1992) Relief, drainage, soil and climate of Ogun State in maps (pp 6–20). In: Onakomaiya SO, Oyesiku OO, Jegede FJ (eds) Rex Charles Publication, Ibadan
- Akintorinwa OJ, Ojo JS, Olorunfemi MO (2011) Appraisal of the cause of pavement failure along the Ilesa–Akure Highway, Southwestern Nigeria using remotely sensed and geotechnical data. *Ife J Sci* 13(1):185–197
- Ako, B.D. (1979): Geophysical prospecting for groundwater in parts of Southwestern Nigeria. Unpublished PhD Thesis. Department of Geology, University of Ife, Ile-Ife, Nigeria, p 371
- Aladejana JA, Talabi AO (2013) Assessment of groundwater quality in Abeokuta, Southwestern Nigeria. *Int J Eng Sci* 2(6):21–31
- ASTM D4318-ITEL (2017): Standard Test methods for liquid limit, plastic limit and plasticity index of soils. ASTM International, West Conshohocken, PA. www.astm.org
- ASTM D4959-07 (2007) Standard test method for determination of water (moisture) content soil by direct heating. Annual Book of ASTM standards. American society for Testing Materials, New York
- ASTM G57-05 (2005) Standard test method for measurement of soil resistivity using two electrode soil box method. Annual Book of ASTM standards. American Society for Testing Materials, New York
- Ayoubi S, Khormah F, SahrawatRodrigues de lima KIAC (2011) Assessing impacts of land use change on soil quality indicator in a loessial soil in Golestan Province. *Iran J Agric Sci Technol* 13:727–742
- Badmus BS, Olatinsu OB (2010) Aquifer characteristics and groundwater recharge pattern in a typical basement complex, Southwestern, Nigeria. *Afr J Environ Sci Technol* 4(6):328–342
- Benderitter Y, Schott JJ (1999) Short-time variation of the resistivity in an unsaturated soil: the relationship with rainfall. *Eur J Environ Eng Geophys* 4:37–49
- Camarero PL, Moreira CA (2017) Geophysical investigation of earth dam using the electrical tomography resistivity technique, REM. *Int Eng J* 70(1):47–52
- Chukka D, Chakravarthi VK (2012) Evaluation of properties of soil subgrade using dynamic cone penetration index—a case study. *Int J Eng Res Dev* 4(4):07–15
- Cook FJ, McQueen DJ, Hart PBS (1986) Physical properties of surface soil in a topsoil removal area and a nearby undisturbed site. *N Z J Agric Res* 29(1):137–142. <https://doi.org/10.1080/00288233.1986.10417986>
- Dafalla MA, Al-Fouzan FA (2012) Influence of Physical parameters and soil chemical composition on Electrical Resistivity. A guide for geotechnical soil profiles. *Int J Electrochem Sci* 7:3191–3204
- Danielsen BE, Dahlin T (2009) Comparison of geo-electrical imaging and tunnel documentation at the Hallandas Tunnel, Sweden. *Eng Geol* 107(3–4):118–129
- De Freitas MH (2009) The basis of engineering geology. In: de Freitas MH (ed) Engineering geology. Springer, Berlin. Doi: https://doi.org/10.1007/978-3-540-68626-2_1.
- Devendran A, Rosli S, Zuhar ZT, Mohammed N (2003) Mapping quarterly sediments using shallow seismic survey USM. Seminar on geo-physics, pp 48–53
- Donohue S, Long M, O'Connor P, Eide-Helle T, Pffathuber AA, Romoen M (2012) Geophysical mapping of quick clay: a case study from Smørgrav, Norway Near Surf Geophys 10(3):207–219
- Doser DI, Dena-Ornelas OS, Langford RP, Baker MR (2004) Monitoring yearly changes and their influence on electrical properties of the shallow substance at two sites near the Rio Grande, West Texas. *J Environ Eng Geophys* 9:179–190
- Egwoonwu GN, Osazuwa IB (2011) Geophysical and geotechnical investigation of the origin of structural instabilities shown on some low rise buildings in Zaria. *Northwest Nig Pacific J Sci Technol* 12(2):534–547
- Essenwanger OM (2003) Classification of climates. Elsevier, Amsterdam
- Ezersky M, Eppelbaum L (2017) Geophysical monitoring of underground constructions and its theoretical basis. *Int J Georesour Environ* 3(2):56–72
- Ezersky M, Legchenko A, Eppelbaum L, Al-Zoubi A (2017) Overview of the geophysical studies in the Dead Sea coastal area related to evaporate karst and recent sinkhole development. *Int J Speleol* 46(2):277–302
- Federal Ministry of Works and Housing (2000) Specification for roads and bridges, vol 2, 271 pp
- Fehdi C, Baali F, Boubaya D, Rouabhiia A (2011) Detection of sinkholes using 2D electrical resistivity imaging in the cheria Basin (North-East of Nigeria). *Arab J Geo Sci* 4:181–187. <https://doi.org/10.1007/s12517-009-0117-2>
- Gardi SQS, Al-heety AJ, Mawlood RZ (2017) Engineering site investigation using 2D electrical resistivity tomography at the Siktan proposed dam site at Erbil governorate, Iraqi Kurdistan. *Reg J Univ Duhok* 21(1):142–154
- Gbadebo AM, Oyedepo JA, Taiwo AM (2010) Variability of nitrate in groundwater in some parts of Southwestern Nigeria. *Pac J Sci Technol* 11(2):572–584
- Gee GW, Or D (2002) Particle size Analysis. In: Dane JH, Topp GC (eds) Methods of soil analysis, part 4, physical methods. SSSA, Madison, pp 255–294
- Grossman RB, Reinsch RC (2002) Bulk density and linear extensibility: core methods. In: Dane JH, Topp GC (eds) Methods of soil analysis, part 4, physical methods. SSSA, Madison, pp 208–228
- Hall KT, Crovetti JA (2007) Effects of subsurface drainage on pavement performance: analysis of the SPS-1 and SPS-2 Field sections. *Trans Res Board* 583:190. <https://doi.org/10.1722/23148>
- Hebbache K, Mellas M, Boubaya D (2016) Application of 2D subsurface electrical resistivity tomography to detect the underground cavities. A case site study: Togla Area (Algeria). *Courr Savoier* 21:33–38
- Hillel D (2004) Introduction to experimental soil physics. Elsevier, London
- Igwe CA, Zarei M, Stahr KK (2013) Soil hydraulic and physic chemical properties of ultisols and inceptisols in south eastern Nigeria. *Arch Agron Soil Sci* 59(4):491–504
- Jegede G (2000) Effect of soil properties on pavement failures along the F209 highway at Ado-Ekiti, southwestern Nigeria. *Constr Build Mater* 14:311–315

- Jones HA, Hockey RD (1964) The geology of southwestern Nigeria. *Geol Surv Niger Bull* 31:22–24
- Kehinde-Phillips O (1992) Geology of Ogun State. In: Onakomaiya SO, Oyesiku OO, Jegede FJ (eds) *Ogun State in Maps*. Rex Charles Publication, Ibadan
- Key R (1992) An introduction to the crystalline basement of Africa. In: Wright E, Burgass W (eds) *Hydrogeology of the crystalline basement aquifers in Africa*, vol 66. Geological society of special publication, London, pp 29–57
- Kiehl JT, Briegleb BP (2011) Pavement surface condition field rating manual for asphalt pavement. *ARPN J Sci Technol* 2(1):17–25
- Kumar, P., Gupta, A. (2010): Case studies of bituminous pavements. *Compendium of papers from the first international conference on pavement preservation*, chap 7, vol 52, pp 505–518
- Livneh M, Ishai I (1987) Pavement and materials evaluation by a dynamic core penetrometer. In: *Proceedings of sixth international conference structural design of Asphalt pavement vol 1*, pp 665–676, Ann Arbor, Michigan, USA, 13–17 July 1987
- Loke, M.H. (2008): RES2DINV- Rapid 2D resistivity and IP inversion using the least square method. *Geo-electrical ranging 2D and 3-D GEOTOMO software*, Malaysia, 145 pp. <https://www.aarhusgeosoftware.dk/res2dinv>.
- Loke MH, Barker RD (1996) Rapid least square in version of apparent resistivity pseudo section by quasi newton method. *Geophys Prospect* 44(1):131–152
- Loke MH, Lane J, John W (2004) Inversion of data from electrical resistivity imaging surveys in water covered areas. *Explor Geophys* 35(4):266–271
- Long M, Donohue S, L'heureux JS, Solberg LL, Ronning JS, Limacher R, O'Connor P, Sauvin G, Romoen M, Leconte I (2012) Relationship between electrical resistivity and basic geotechnical parameters for marine clays. *Can Geotech J* 49:1158–1168. <https://doi.org/10.1139/T2012-080>
- Maslakowski M, Kowalczyk S, Mieszkowski R, Jozefiak K (2014) Using electrical resistivity tomography (ERT) as a tool in geotechnical investigation of the substrate of a highway. *Stud Quat* 31(2):83–89
- Materchera SA (2018) Soil properties and subsoil constraints of urban and peri-urban agriculture within Mahikeng city in the North West Province (South Africa). *J Soils Sediments* 18:494–505. <https://doi.org/10.1007/s11368-016-1569-0>
- Mesida EA (1987) The relationship between the geology and the lateritic engineering soils in the northern environs of Akure, Nigeria. *Bull Int Assoc Eng Geol* 35:65–69
- Mocnik A, Dossi M, Forte E, Zambrini R, Zamariolo A, Pipan M (2015) Ground penetrating radar applications for roads and airport pavements investigations. *GNG TS Sess* 3(2):106–112
- Momoh LO, Akintorinwa O, Olorunfemi MO (2008) Geophysical investigation of highway failure—a case study from the basement complex terrain of Southwestern Nigeria. *J Appl Sci Res* 4(6):637–648
- NGSA (2016) Geological and mineral resources map of Ogun State. Nigerian Geological Survey Agency, Nigeria
- ODOT (2002) The 2002 construction and material specification Office of Construction Administration. Ohio DOT, Columbus
- Okpoli CC (2014) 2D resistivity imaging and geotechnical investigation of structural collapsed lecture theatre in Adekunle Ajasin University, Akungba-Akoko, Southwestern Nigerian. *Environ Res Eng Manag* 3(69):49–59
- Okpoli CC, Bamidele AA (2016) Geotechnical investigation and 2D electrical resistivity survey of a pavement failure in Ogbagi road, southwestern, Nigeria. *Int Basic Appl Res J* 2(7):47–58
- Oladapo MI, Olorunfunmi MO, Ojo JS (2008) Geophysical investigation of road failure in a basement area of southwestern. Nigeria *Res J Appl Sci* 3(2):103–112
- Oladunjoye MA, Salami A, Aizebeokhai J, SanuadeKaka OASI (2017) Preliminary geotechnical characterization of a site in southwest Nigeria using integrated electrical and seismic methods. *J Geol Soc India* 89:209–215
- Olofinyo OO, Olabode OO, Fatoyinbo IO (2019) Engineering properties of residual soils in parts of Southwestern Nigeria: Implication for road foundation. *SN Appl Sci* 1:507. <https://doi.org/10.1007/s42452-019-0515-3>
- Oloruntola MO, Adeyemi GO (2014) Geophysical and hydro-chemical evaluations of groundwater potential and character of Abeokuta Area, southwestern Nigeria. *J Geogr Geol* 6(3):162–177
- Omisore, B.O., Olorunfemi, M.O. and Sheng, J. (2016): Geo-electric investigation of a proposed Mambilla plateau Airport runway, Taraba state, Nigeria. In: *Seventh international conference on environmental and engineering geophysics and summit forum of Chinese Academy of engineering on engineering science and technology*, pp 243–246
- Oni AG, Olorunfemi MO (2016) Integrated geophysical investigation of the Igbara-Oke-Igbara-Odo road pavement failure in Ondo/Ekiti State, Southwestern Nigeria. *Ife J Sci* 18(1):119–131
- Onuoha DC, Onwuka SU (2014) The place of soil geotechnical characteristics in road failure, a study of the Onitsha–Enugu expressway, south-eastern Nigeria. *Int J Sci Technol* 1:55–67
- Osemudiamen, V.E. (2013): Geophysical investigation of road failure using electrical resistivity imaging method, A case study of Uhiele–Opaji Road, Edo State. Unpublished M.Sc Thesis. Department of Geology, University of Nigeria, Nsukka, 128 pp
- Osinowo OO, Akanji AO, Adewale A (2011) Integrated geophysical and geotechnical investigation of the failed portion of a road in basement complex terrain, southwest Nigeria. *RMZ Mater Geoenviron* 58(2):143–162
- Oyeyemi KD, Aizebeokhai AP, Adagunodo TA, Olofinnade OM, Sanuade OA, Olajojo AA (2017) Subsoil characterization using geoelectrical and geotechnical investigation: implications for foundation studies. *Int J Civil Eng Technol* 8(10):302–314
- Ozegin KO, Adetoyinbo AA, Jegede SI, Ogunseye TT (2016) Troubled roads: Application of surface geophysics to highway failures of the sedimentary terrain (Irukekpen–Ifon Road) of Edo State, Nigeria. *Int J Phys Sci* 11(22):296–305. <https://doi.org/10.5897/IJPS2016.4546>
- Peter JE, Rafiu AA, Udensi EE, Salako KA, Alhassan UD, Adetona AA (2018) 2D Electrical Resistivity Imaging investigation on causes of road failure along Kutigi Street, Minna North Central Nigeria. *Am J Innov Res Appl Sci* 6(5):221–226
- Reynolds WD, Elrick DE (2002) Constant head soil core (tank) method. In: Dane JH, Topp GC (eds) *Methods of soil analysis*, part 4, physical methods, Wisconsin, pp 804–808
- Saarenketo T, Scullion T (2000) Road evaluation with ground penetrating radar. *J Appl Geophys* 43:119–138
- Samouëlian A, Cousin I, Tabbagh A, Bruand A, Richard G (2005) Electrical resistivity in soil science: a review. *Soil Tillage Res* 83:173–193. <https://doi.org/10.1016/j.still.2004.10.004>
- Sasaki Y (1992) Resolution of resistivity tomography inferred from numerical simulation. *Geophys Prospect* 40:453–464
- Shaaban F, Ismail A, Massoud U, Mesbah H, Lethy A, Abbas AM (2013) Geotechnical assessment of ground conditions around a titled building in Cairo–Egypt using geophysical approaches. *J Assoc Arab Univ Basic Appl Sci* 13:63–72
- Shukla MK, Lal R, Ebinger M (2006) Determining soil quality indicators by factor analysis. *Soil Tillage Res* 87:194–204
- Singh D, Jha JN, Gill KS (2016) Strength evaluation of soil subgrade using in-situ tests. *Civil Eng Architect* 4(6):201–212. <https://doi.org/10.13189/cea.2016.040601>
- Soupios PM, Georgakopoulos P, Papadopoulos N, Saltas V, Andreadakis A, Vallianatos F, Sarris A, Makris JP (2007) Use of

- engineering geophysics to investigate a site for a building foundation. *J Geophys Eng* 4:94–103
- Ufoegbune GC, Lamidi KI, Awomeso JA, Eruola AO, Idowu OA, Adeofun O (2009) Hydrogeological characteristics and groundwater quality assessment in some selected communities of Abeokuta, southwestern Nigeria. *J Environ Chem Ecotoxicol* 1(1):10–22
- Vaitkus A, Žalimienė L, Židanavičiūtė J, Žilionienė D (2019) Influence of temperature and moisture content on pavement bearing capacity with improved subgrade. *Materials (Basel)* 12(23):3826. <https://doi.org/10.3390/ma12233826>
- Van der Velpen, B.P.A (1998): RESIST Version 1.0. a package for the processing of the resistivity sounding data . M.Sc Research Project. ITC, Delft, The Netherlands
- Van der Velpen, B.P.A. (2004): WINRESIST Version 1.0 Resistivity Depth Sounding interpretation software. MSc Research Project, ITC, Delft, The Netherlands
- Vanags, C., Minasny, B., McBratney; A.B. (2004): The dynamic penetrometer for assessment of soil mechanical resistance supersoil 2004. In: Third Australian New Zealand soils conference, 5–9 Dec 2004. University of Sydney, Australia Published on CDRom, pp 1–8. www.regional.org.au/au/assi/
- Vogelmann ES, Reichert JM, Reinert DJ, Mentges MI, Vieira DA, Peixoto de Barros CA, Fasinmirin JT (2010) Water repellency in soils of humid subtropical climate of Rio Grande de sul, Brazil. *Soil Tillage Res* 110:126–133
- Wu S, Sargand S (2007) Use of dynamic core penetrometer in subgrade and base acceptance. Ohio University, Ohio Research Institute for Transportation and the Environment, Stocker Centre, IYI, Athens, Ohio 45701-2979. 124pgs. Reports No: FHWA/ODOT-2007/01
- Xu Y, Sun L (2013) Study on pavement deformation of asphalt mixtures by single penetration repeated shear test. *Proc Soc Behav Sci* 96:886–893
- Yuejian C, Guzina BB, Labuz JF (2008) Pavement evaluation using ground penetrating radar. Minnesota Department of Transportation, St. Paul
- Zheng Y, Zhang P, Liu H (2019) Correlation between pavement temperature and deflection basin form factors of asphalt pavement. *Int J Pavement Eng* 20:874–883. <https://doi.org/10.1080/10298436.2017.1356172>
- Žiliūtė L, Motiejūnas A, Kleizinė R, Gribulis G, Kravcovas I (2016) Temperature and moisture variation in pavement structures of the test road. 6th Transport Research Arena, April 18–21. *Transp Res Proc* 14:778–786
- Zou G, Xu J, Wu C (2017) Evaluation of factors that affecting rutting resistance of asphalt mixes by orthogonal experiment design. *Int J Pavement Res Technol* 10:282–288

Publisher's Note Springer Nature remains neutral with regard to jurisdictional claims in published maps and institutional affiliations.

Authors and Affiliations

S. A. Ganiyu¹  · M. A. Oladunjoye² · M. O. Olobadola¹ · A. P. Aizebeokhai³ · B. S. Badmus¹

¹ Department of Physics, Federal University of Agriculture, Abeokuta, Ogun, Nigeria

² Department of Geology, University of Ibadan, Ibadan, Ogun, Nigeria

³ Department of Physics, Covenant University, Ota, Ogun, Nigeria